A Nanoparticle-Decorated Biomolecule-Responsive Polymer Enables Robust Signaling Cascade for Biosensing

*Zuan-Tao Lin, Jianhua Gu, Chien-Hung Li, T. Randall Lee, Lixin Xie, Shuo Chen, Piao-Yang Cao, Shan Jiang, Yulin Yuan, Xia Hong, Hongting Wang, Dezhi Wang, Xifan Wang, Gang-Biao Jiang, Mikala Heon, and Tianfu Wu**

To meet the increasing demands for ultrasensitivity in monitoring trace amounts of low-abundance early biomarkers or environmental toxins, the development of a robust sensing system is urgently needed. Here, a novel signal cascade strategy is reported via an ultrasensitive polymeric sensing system (UPSS) composed of gold nanoparticle (gNP)-decorated polymer, which enables gNP aggregation in polymeric network and electrical conductance change upon specific aptamer-based biomolecular recognition. Ultralow concentrations of thrombin (10^{-18} M) as well as a low molecular weight anatoxin (165 Da, 10^{-14} M) are detected selectively and reproducibly. The biomolecular recognition induced polymeric network shrinkage responses as well as dose-dependent responses of the UPSS are validated using *in situ* real-time atomic-force microscopy, representing the first instance of real-time detection of biomolecular binding-induced polymer shrinkage in soft matter. Furthermore, *in situ* real-time confocal laser scanning microscopy imaging reveals the dynamic process of gNP aggregation responses upon biomolecular binding.

The early detection of pathogens, biomarkers, or toxins in clinical or environmental samples is a great challenge, especially at ultralow concentrations.[1,2] Conventional technologies using cell culture, polymerase chain reaction, chromatography/mass spectrometry, or enzyme-linked immunosorbent assay are tedious, time consuming, and rely heavily on expensive and sophisticated instruments, antibodies, and well-trained personnel.[3,4] Therefore, there is an increasing demand to develop a facile and rapid sensing strategy to tackle these challenges. So far, the most successful commercial application of a bioanalytic sensor is the personal blood glucose detector.[5] Since then, there have been many efforts in building various biosensors.[2,6,7] The greatest challenge for single-biomolecule detection is the relatively limited signal amplification capability in current biosensors.[8] Recently, considerable progress has been made in the synthesis of functionalized macromolecule.[3,6,9] Signal amplification based on macromolecule and electrical devices has drawn tremendous attention in improving the sensitivity of biosensors.[3,8,10] However, most of these biosensors are unsatisfactory in sensitivity or ease-of-use, which has largely precluded the possibility of their use for field applications.[11] Polymer consisting of a polymeric network via cross-linking monomers or molecularly functionalized monomers can be used to fabricate highly responsive sensors.[6,12,13] Importantly, polymer-based sensors have shown good potential for signal amplification.[3,6] However, their performance in precise quantification is typically inadequate.

Aptamers are oligonucleotides capable of binding small molecules, proteins, or nucleic acids with high affinity[14] and have great potential in building specific biosensors due to their selectivity and thermal stability. Electrical sensors are portable and offer potential for use in point-of-care applications.[15] Since gold nanoparticles (gNPs) possess unique electrical, and optical, as well as facile surface modification, the nanomaterials can be potentially used in electrical biosensors if integrated into cross-linked polymeric network.[16] We hypothesize that the

Z.-T. Lin, Prof. S. Jiang, Dr. Y. Yuan, Prof. X. Hong, Dr. H. Wang, Prof. G.-B. Jiang, M. Heon, Prof. T. Wu
Department of Biomedical Engineering
University of Houston
Houston, TX 77204, USA
E-mail: twu13@central.uh.edu

Dr. J. Gu
Electron Microscopy Core
Houston Methodist Research Institute
Houston, TX 77030, USA

Dr. C.-H. Li, Prof. T. R. Lee
Department of Chemistry
University of Houston
Houston, TX 77204, USA

L. Xie, Prof. S. Chen, Prof. D. Wang
Department of Physics and TcSUH
University of Houston
Houston, TX 77204, USA

P.-Y. Cao, Prof. G.-B. Jiang
College of Materials and Energy
South China Agricultural University
Guangzhou 510642, China

X. Wang
Department of Materials Science and NanoEngineering
Rice University
TX 77005, USA

DOI: 10.1002/adma.201702090

incorporation of gNPs into a polymeric biosensor can tremendously amplify polymeric network shrinkage signals induced by specific aptamer recognition and binding. Here, we designed and fabricated a conceptually novel signal amplification cascade based on a new hybrid polymeric sensor composed of a gNP-decorated chitosan derivative and precisely engineered target-specific aptamer chains and polyacrylamides, which enables a robust assay for ultralow target molecules with high sensitivity and selectivity. The first-step signal amplification is target molecule binding-induced polymeric network shrinkage, followed by a second step signal amplification (conductance change of polymer) in virtue of gNP aggregation caused by polymeric network shrinkage. This novel "signal cascade amplifier" is able to quantitatively detect target molecules at ultralow concentrations by monitoring changes in electrical conductance. The use of *in situ* real-time atomic-force microscopy (AFM) and confocal laser scanning microscopy (CLSM) imaging allowed us to determine and understand the structure and dynamics of this new ultrasensitive polymeric sensing system (UPSS) on target molecule binding at microstructural levels.

The design and fabrication of the UPSS are presented in **Figure 1**. To immobilize gNPs within the UPSS, we synthesized a composite of thioglycolic acid and chitosan (TGA–chitosan) to bind the gNPs. The Fourier transform infrared (FT-IR) and ^{1}H NMR spectra of chitosan and TGA–chitosan shown in Figures S1 and S2 (Supporting Information) demonstrated that the thiol groups were conjugated onto the amine groups of chitosan successfully. To verify the covalent attachment of thiol groups of TGA–chitosan onto the surface of gNPs, we analyzed the S 2p region of the X-ray photoelectron spectroscopy (XPS) spectra of TGA–chitosan and gNP-decorated TGA–chitosan. The interactions between gNPs and thiol groups of TGA–chitosan are shown in **Figure 2**a. The peak in the S 2p spectra can be deconvoluted as doublet with a branching ratio of 1:2 and a splitting of 1.2 eV.[17] As shown in Figure 2b, in the spectrum of TGA–chitosan, the S 2p peak was deconvoluted to 164.5 and 163.3 eV (S $2p_{1/2}$ and S $2p_{3/2}$), and we assigned these peaks to the unbound sulfur of the thiol group by referencing to the Au $4f_{7/2}$ peak at 84.0 eV (see Figure S3 in the Supporting Information). Upon binding to the surface of gNPs, the corresponding S 2p peak shifted to 163.7 and 162.5 eV (Figure 2b, bottom), confirming that the gNPs were immobilized on the backbone of TGA–chitosan.[17] In addition, Figure 2b (bottom) shows a very small peak at 164.4 eV in the spectrum of gNP-decorated TGA–chitosan, consistent with a model in which the preponderance of the thiol groups were bound to the surface of the gNPs.[17]

Transmission electron microscopy (TEM) images of gNP-decorated TGA–chitosan and the polymeric sensor are shown in Figure 2c–h. The morphology of the gNPs is approximately spherical, and the size of the TGA–chitosan conjugated gNPs ranges between 2 and 5 nm. By using a hollow grid, we could observe the gNP-decorated TGA–chitosan on the edge of the carbon grid (Figure 2f), illustrated in Figure 2e. TEM images of the gNP-decorated polymeric sensor under different magnifications are shown in Figure 2g,h. Cross-sectional scanning electron microscope (SEM) imaging was also used to demonstrate the microstructure of the polymeric sensor as shown in Figure S4 (Supporting Information).

Figure 2i displays a schematic illustration of the interactions between AFM probe and the surface of polymeric sensor. Compared to the soft and adhesive property of polymer, the metal properties of gNPs exhibited stiffness in the force spectroscopy of AFM. As demonstrated in Figure 2j–l, the height (Figure 2j), log dilatometer test (DMT) modulus (Figure 2k), and adhesion (Figure 2l) images could be obtained for the polymeric sensor. Because of the attachment of polymer to the gNPs, the sizes of the gNPs observed in the height images were larger than those in the TEM images (Figure 2c,d,f–h), which might arise from the convolution effect of the AFM tip. To confirm that the peaks in the surface topography represent gNPs, Log DMT Modulus, and adhesion images were used to analyze the stiffness and adhesion of the polymer surface. The corresponding positions in the Log DMT Modulus and adhesion images displayed "high" for stiffness and "low" for adhesion, which is consistent with the position of gNPs in the height images. As expected, the softness and high adhesion properties of the polymer matrix were observed in these AFM images. The number of gNPs can be quantified from the Log DMT Modulus and adhesion images in the corresponding positions.

Next, we employed CLSM to observe the biomolecular structure and distribution of biomolecular recognition cores inside the polymeric sensor. As illustrated in **Figure 3**a,b, the thrombin-specific polymeric sensor was fabricated by fluorescently labeled human thrombin aptamer-2 (Alexa Fluor 647, red), and the template thrombin was stained with fluorescein isothiocyanate (FITC)-labeled anti-human IgG antibody. Thrombin (Figure 3c) and aptamers (Figure 3d) were uniformly distributed in the polymeric network (Figure 3e). In contrast, there was no green fluorescence found in the negative control groups, either in the absence of target molecules (Figure 3f) or stained with sheep IgG isotype control (Figure 3g). To explore further the spatial distribution of the biomolecular recognition core in the polymeric sensor, 3D CLSM images were obtained (Figure 3h–j), where thrombin (green) molecules were surrounded by fluorescently labeled aptamers (red).

Taking advantage of the autofluorescence of gNPs, we monitored the real-time aggregation of the gNPs upon biomolecular recognition using in situ CLSM. To investigate the dynamics of gNP responses in the UPSS, 200 nm gNPs were used to build the thrombin-specific polymeric sensor for visualization under CLSM. As shown in **Figure 4**a, when target molecules were bound to biomolecular recognition cavities, the polymeric network shrank followed by the reduction of the distances between gNPs. As shown in Figure 4b, numerous gNPs were bound to the long backbone chain and aggregated on TGA–chitosan, and the distance between gNPs was significantly shortened upon the addition of 1×10^{-16} M thrombin solution, resulting in the aggregation of gNPs within a polymer (Figure 4b and Movie S1 (Supporting Information)). However, no aggregation of gNPs was observed upon the addition of phosphate buffered saline (PBS) (Figure 4b and Movie S1 (Supporting Information)). This observation is in agreement with the result from the real-time *in situ* AFM study described below.

To investigate further the dynamics of polymeric network shrinkage using AFM, the topography and height profiles were recorded and analyzed during polymeric network shrinkage in response to PBS or thrombin, as illustrated in Figure 4c. We

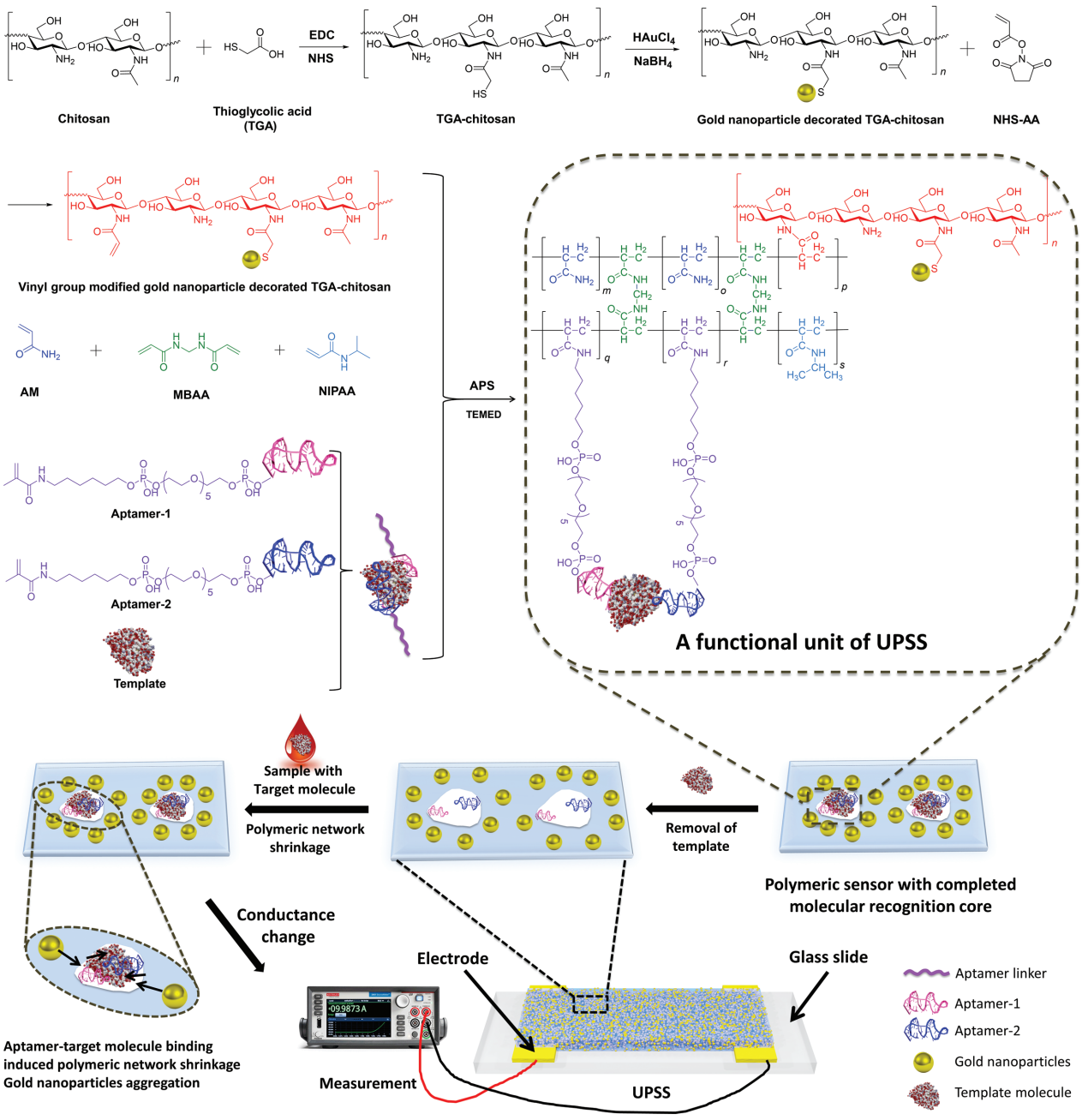

Figure 1. Design and fabrication of an ultrasensitive polymeric sensing system (UPSS). TGA–chitosan was synthesized via the conjugation of TGA onto chitosan. Gold nanoparticle (gNP)-decorated TGA–chitosan was then synthesized and immobilized into the polymeric network. A molecular recognition core composed of a pair of target-specific aptamers and the template molecules was incorporated into the polymeric sensor. A molecularly imprinted cavity harboring a pair of aptamers specific for the target molecule was generated by removing the template molecules. Biomolecular recognition-induced polymeric network shrinkage of the polymeric sensor shortened the distance between the gNPs, resulting in the aggregation of gNPs within the polymer, and subsequently changed the electrical conductance of the polymeric sensor. The conductance was determined using a source meter.

selected two natural land markers A and B in the polymeric sensor, corresponding to "A" and "B" on the topography image and cross-sectional height profile (Figure 4c–e). Upon the addition of PBS to the polymeric sensor, there was no change in the distance between the two land markers A and B as shown in the cross-sectional height profile; however, significant shrinkage was observed upon the addition of thrombin. The distance between A and B was 20.3 µm upon the addition of thrombin, representing 4.7% shrinkage (Figure 4e).

To test the sensitivity and specificity of the UPSS, human α-thrombin or ATXa were used as template molecules. The binding isotherm of thrombin for polymeric sensor was carried out in the presence of various concentrations of thrombin ranging from 1×10^{-21} to 1×10^{-6} M in PBS or artificial urine.

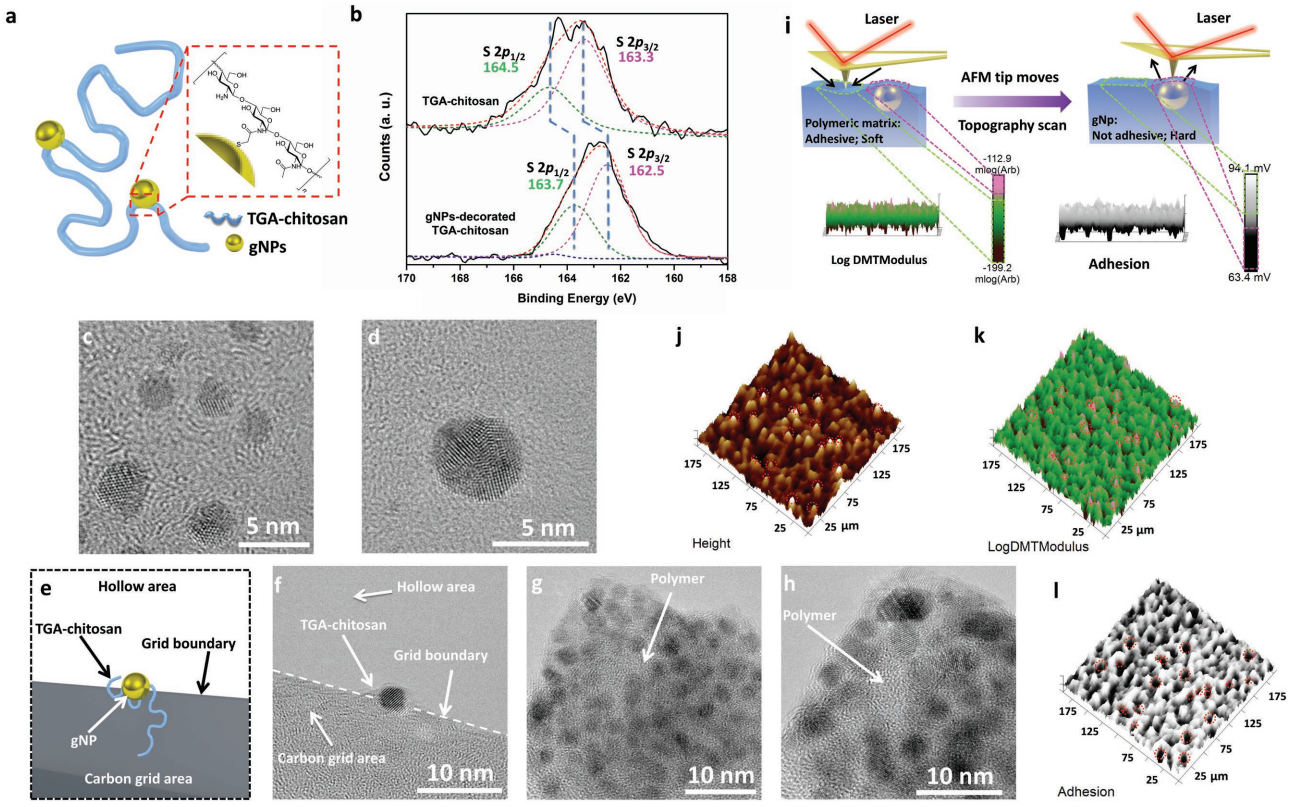

Figure 2. Characterization of UPSS. a) XPS spectra of S 2p region of TGA–chitosan before and after being decorated with gNPs: The unbound S 2p peak appeared between 163 and 165 eV; after being bound to gNPs, the S 2p peak shifted to 162 and 164 eV. b) The interactions between the gNPs and thiol groups of TGA–chitosan are illustrated. TEM images of the gNP of c,d) gNP-decorated TGA–chitosan as well as g,h) the polymeric sensor are shown. The range of the gNP size is 2–5 nm. e–h) A hollow grid was used to visualize the TGA–chitosan and polymer sensor. The schematic illustration of TGA–chitosan-decorated gNPs on a TEM hollow grid is shown in (e). The scheme of i) the mechanism of AFM surface scan and the topography of the polymeric sensor are shown, and j) the height mode shows the topography of the polymeric sensor and the gNPs can be observed as circled. The corresponding k) Log DMT Modulus and l) adhesion modes could differentiate the gNPs and polymeric matrix.

As shown in **Figure 5**a,b, the limit of detection (LOD) for human α-thrombin reached 10^{-18} M in both PBS and artificial urine. The highest electrical conductance change for thrombin detection in PBS and artificial urine solution were 118.5 ± 5.0% and 82.2 ± 2.3%, respectively. In addition, this polymeric sensor demonstrated excellent selectivity: the electrical conductance change was at baseline levels upon the addition of negative controls such as bovine serum albumin (BSA) or bovine thrombin in the human α-thrombin-specific UPSS (Figure 5a,b).

We also tested the feasibility of using the UPSS to detect one of the cyanotoxins, anatoxin a (ATXa). The electrical conductance changes that the UPSS produces vary linearity with the concentration of ATXa in the range of 10^{-15}–10^{-10} M and the LOD was 10^{-14} M as shown in Figure 5c. The ATXa-specific UPSS did not respond to two other cyanotoxins, cylindrospermopsin, and brevetoxin-2 (BTX-2), indicating that the ATXa-specific UPSS is selective.

Real-time in situ AFM imaging was applied to measure the dynamic responses of the polymeric sensor. As shown in Figure 5d, upon the binding of target molecules, the polymeric network starts to shrink and generates a displacement Δx. The frictional force between the AFM probe tip and the polymeric surface causes the tip to move, resulting in a displacement of Δx. The lateral force, L, caused by the corresponding torsional deformation of the cantilever can be measured by the AFM and is proportional to the displacement Δx. The lateral force (expressed as "output signal" in AFM) change was dose dependent upon biomolecular recognition and binding (Figure 5e). When the polymeric sensor was incubated with PBS, the frictional force remained flat within 10 min. In contrast, the frictional force increased significantly in a dose-dependent manner with increasing thrombin concentrations over time upon target binding.

We carefully examined the impact of the building blocks of the UPSS on its functionality. Briefly, we examined how various concentrations of methylenebisacrylamide (Figure S5a, Supporting Information), *N*-isopropyl acrylamide (NIPAA) (Figure S5b, Supporting Information), gNPs (Figure S6, Supporting Information), and aptamers (Figure S7, Supporting Information) as well as the size of gNP (Figure S8, Supporting Information) impact the functionality of the UPSS, and we identified optimal conditions for the best performance of the UPSS.

UV–vis study suggests that more than 97% of the aptamers were incorporated into the UPSS, see Figure S9 (Supporting Information).

We then visualized and quantified the thrombin binding dynamics (Figure 5f–n), where the ratio of green fluorescence

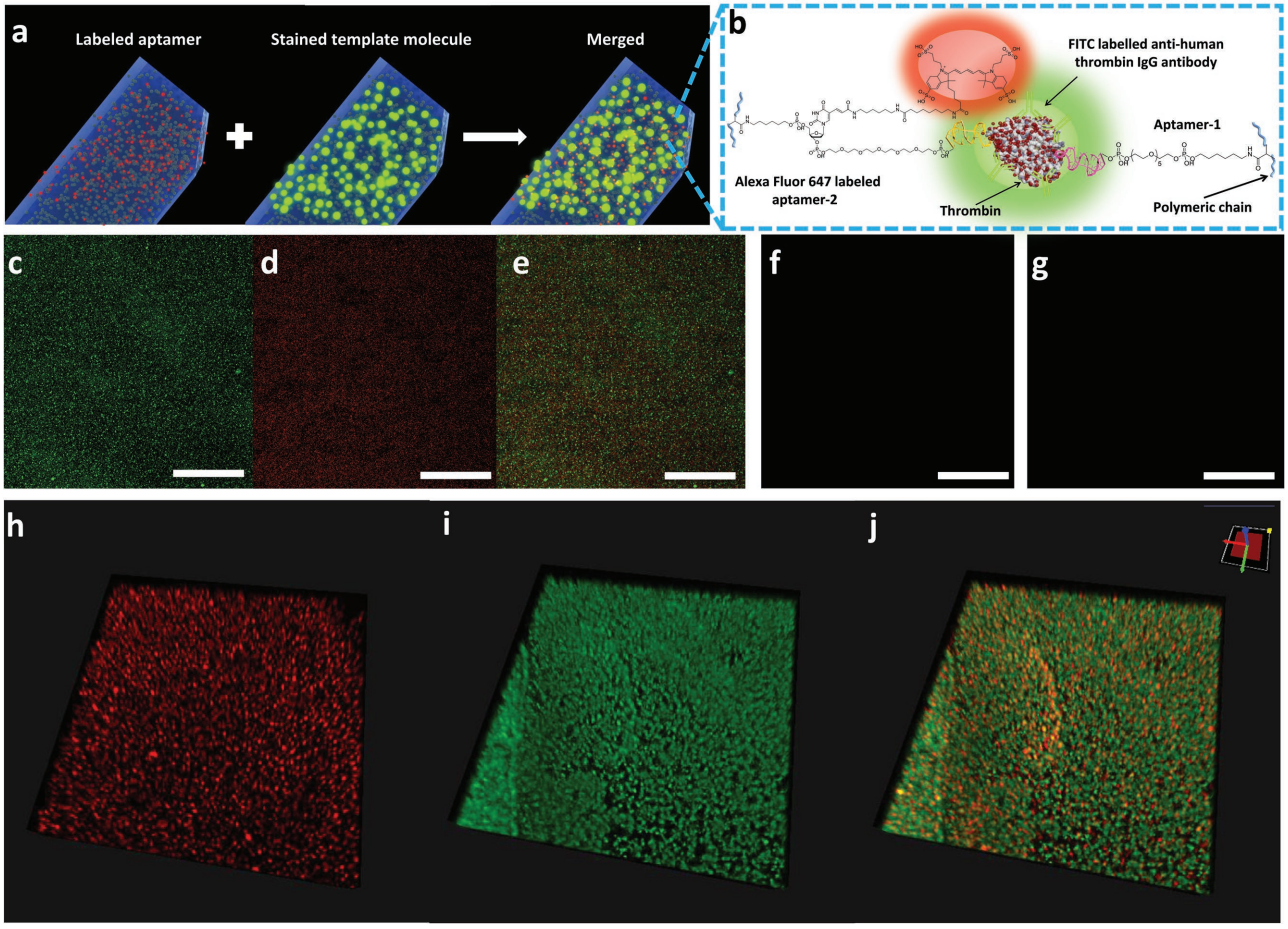

Figure 3. Visualization of the biomolecular recognition cores within UPSS using CLSM. In the polymeric sensor, the template molecule thrombin was bound by a pair of thrombin-specific aptamers where a fluorescent dye was conjugated to the oligo via *N*-hydroxysuccinimide (NHS) ester chemistry on a "T" base. A scheme of the polymeric sensor displays the decorated gNPs, template-specific aptamers (fluorescently labeled in red), and template molecules (bond to fluorescently labeled antibody), where a) the merged image is shown, and b) the labeling strategies are shown. c–g) 2D confocal images of the polymeric sensor are shown, where the template molecules were stained with FITC-labeled anti-human thrombin IgG antibody (green, c), the aptamer was Alexa Flour 647 labeled (red, d), and the merged biomolecular recognition core (e). Negative controls, either in the absence of template molecule (f), or stained with sheep IgG isotype control (g) are included. h–j) 3D confocal images of polymeric sensors are shown. Scale bars (c)–(g): 100 µm.

intensity to red fluorescence intensity of the polymeric sensor were 18.8 ± 2.9%, 57.9 ± 1.8%, and 81.1 ± 2.6%, after incubation with 1×10^{-16}, 1×10^{-12}, and 1×10^{-10} M thrombin, respectively. As expected, the ratio increased with the elevated of thrombin concentration.

As shown in Figure 5o, the complete recognition core complex (G1) with aptamer-1 + template thrombin + aptamer-2 displayed the best performance reflected by electrical conductance change. However, the biomolecular recognition core made of template thrombin and a single aptamer (aptamer-1, G3 or aptamer-2, G4) compromised the robustness of the UPSS. If template thrombin was absent, the functionality of the sensor was partially lost irrespective of the presence of aptamer-1 + aptamer-2 (G2) or single aptamers (G5 and G6). Likewise, the absence of aptamers compromised the functionality of the UPSS (G7). As expected, the UPSS without a biomolecular recognition core (no template thrombin and aptamers) completely lost its functionality (G8). This experiment further demonstrated that both aptamers and template molecules are essential to achieve the best performance as reflected by electrical conductance change. Aptamers in the biomolecular recognition core could significantly improve the selectivity of the sensor compared to previous molecular imprint systems.[18,19]

We then asked if the UPSS assay is reproducible and if the polymeric sensor could be recycled after the first use. Briefly, after two additional binding-removal-rebinding cycles with 1×10^{-8} thrombin, the functionality, and robustness of the UPSS (as reflected by electrical conductance change) remained the same as in the first assay (Figure S10, Supporting Information), indicating reversibility of the biomolecular recognition. Also, the UPSS assay results from three independent experiments indicate that it has good reproducibility.

In this study, we designed and fabricated a highly sensitive and selective UPSS composed of a novel signal amplification cascade system allowing for robust and accurate biomolecular recognition. First, the specific "aptamer-template molecule" complex-based biomolecular recognition cores are the basis for the selectivity and accuracy of the UPSS. Therefore, it is

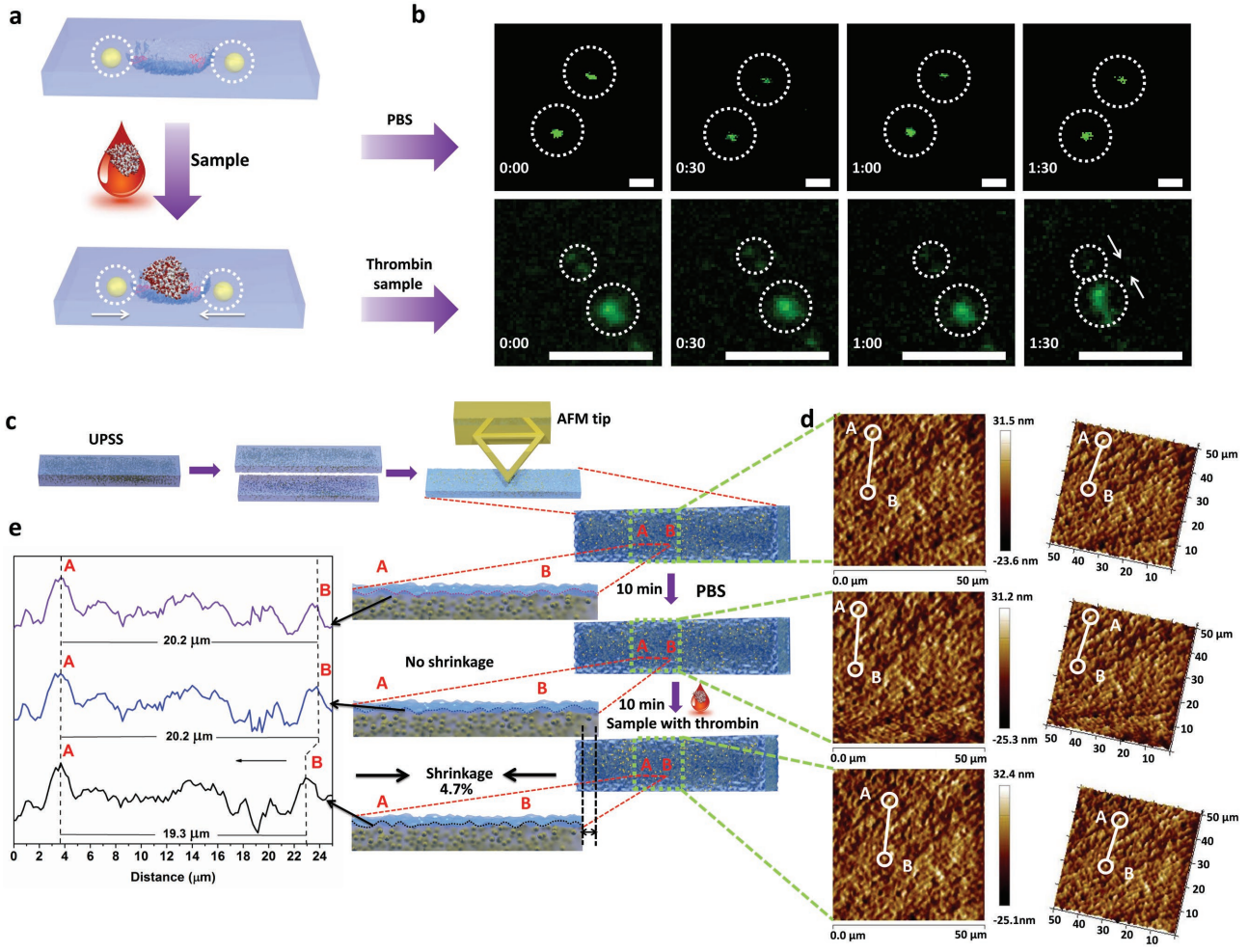

Figure 4. *In situ* CLSM visualization of gNP aggregation in response to biomolecular binding and *in situ* AFM contact mode imaging of UPSS. The distance between gNPs is reduced when the polymeric shrinks, thereby causing an amplified conductance change. Upon excitation, 200 nm gNPs emit fluorescence (at 488 nm), which is visible under a confocal microscope. a) Hence, we could track gNP aggregation upon biomolecular recognition and binding, as illustrated in. Time-lapse CLSM imaging of the dynamic behavior of gNPs upon the addition of 1×10^{-16} M thrombin. b) PBS was used as a negative control, where no responses were observed upon addition (scale bar: 5 µm). c) To detect the shrinkage responses of the thrombin-specific polymeric sensor upon the addition of 1×10^{-8} M thrombin or PBS, the polymer was slated to obtain natural land markers (A and B) on the rough surface. d) *In situ* AFM topography of the polymeric sensor is shown before and after adding PBS or 1×10^{-8} M thrombin. e) The distance change between land marker A and B was derived from (d).

conceptually different from the previous reported biomolecular imprint technologies that on the "memory" of the morphology of template molecules.[19] Second, this polymeric sensor is highly contractible upon biomolecular recognition, thus, the target molecule binding-induced polymeric network shrinkage can serve as the primary responses (first-step signal amplification) of the UPSS. Third, the incorporation of gold nanoparticles into the polymeric sensor allows for a second-step signal amplification, where the conductance change of the polymeric sensor can serve as the final response. This "signal cascade amplifier" significantly increases the sensitivity and robustness of the UPSS as a novel biosensing system. The last few decades have witnessed a wide variety of polymeric sensors with attractive features in signal amplification.[3,6] However, these one-step amplification strategies have greatly compromised the functionality and potential of these sensors toward higher sensitivity or accuracy. To the best of our knowledge, the LOD of our UPSS for thrombin (10^{-18} M) is superior to previous reports in detection of thrombin.[13,20] The LOD for ATXa is 10^{-14} M, which is among the highest sensitivity when compared to the literature or commercial products as summarized in Table S1 (Supporting Information).

Importantly, the report describes for the first time a visualization of dynamic process of target molecule binding-induced aggregation of gNPs using in situ real-time CLSM imaging. We have used 200 nm gNPs to track the UPSS responses triggered by biomolecular recognition and polymeric network shrinkage (Figure 4b and Movies S1 and S2 (Supporting Information)). Also, this report describes the first visualization of the aptamer-protein binding structure and the formation of a biomolecular recognition core inside a polymeric network sensor at a microstructural level using CLSM. The quantification of fluorescent intensity of CLSM images of the polymeric network sensor in response to various concentrations of target molecules was

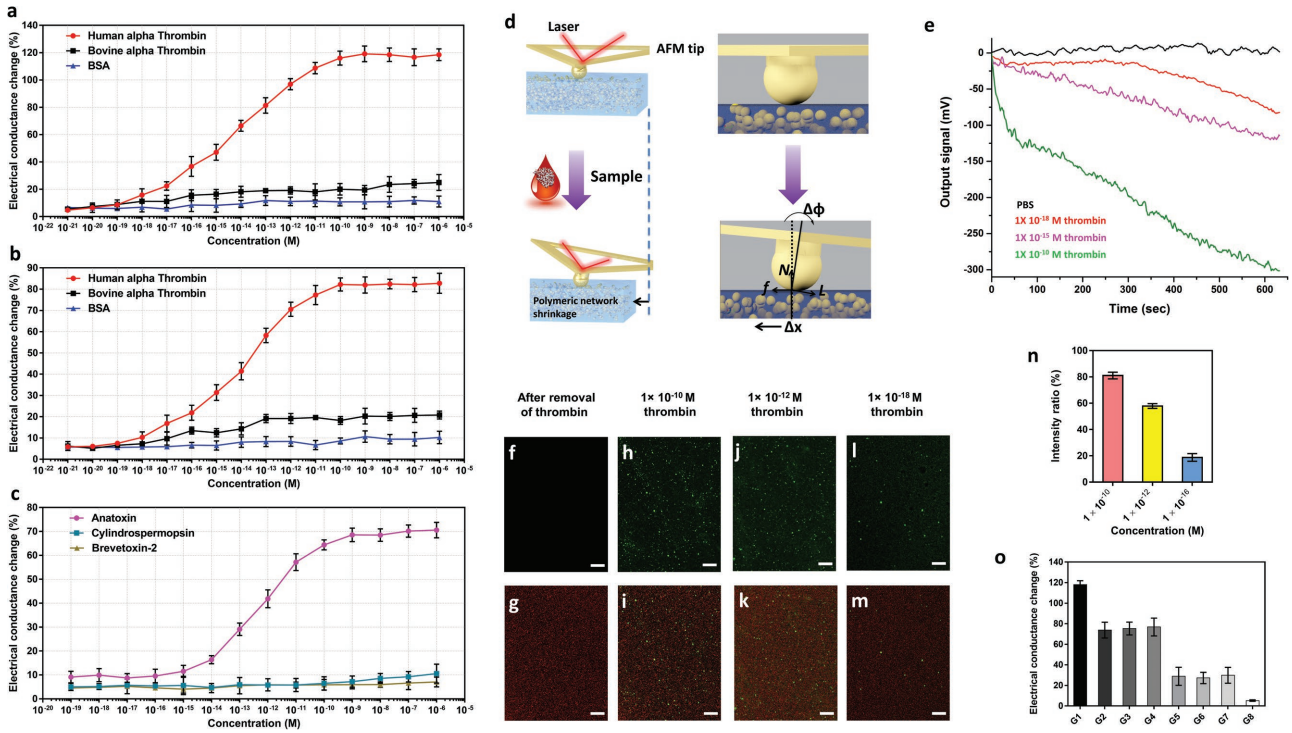

Figure 5. Functionality of UPSS and Dose-dependent responses of UPSS using in situ real-time AFM. a) In a human α-thrombin specific UPSS, dose-dependent responses of UPSS to various concentrations of human α-thrombin, bovine α-thrombin, or BSA were examined to determine the sensitivity and selectivity, using electrical conductance as an output. b) Similar measurements were also performed where various concentrations of human α-thrombin, bovine α-thrombin, or BSA were spiked in artificial urine. c) The kinetics of ATXa binding to an ATXa-specific polymeric sensor was investigated using either cylindrospermopsin or BTX-2 as negative controls. d) Illustration of real-time measurement of polymeric network shrinkage responses upon biomolecular recognition using AFM in contact mode. The polymeric sensor is immobilized by setting the scan size as "0." After adding target molecules, the polymeric network starts to shrink and generates a displacement of Δx. The frictional force between the tip and the polymer surface causes the tip to move with the same amount of displacement Δx. The lateral force, L, caused by the corresponding torsional deformation of the cantilever, can be measured by the AFM and is related to the displacement Δx. e) The results of real-time change of signal output in response to various concentrations of thrombin are shown (black: PBS; red: 1×10^{-18} M thrombin; purple: 1×10^{-15} M thrombin; green: 1×10^{-10} M thrombin). f,g) CLSM image of polymeric sensor after the removal of thrombin template. Green fluorescence and merged CLSM images of the polymeric sensor incubated with h,i) 1×10^{-10} M, j,k) 1×10^{-12} M, and l,m) 1×10^{-16} M thrombin. Scale bar: 10 µm. n) The ratio of green fluorescent intensity to red fluorescent intensity calculated from the CLSM image of polymeric sensor incubated with 1×10^{-10}, 1×10^{-12}, and 1×10^{-16} M thrombin. o) Effect of the components of biomolecular recognition core on the functionality of UPSS upon the addition of 1×10^{-8} M thrombin: the biomolecular recognition core was fabricated with both thrombin aptamer pair and the template thrombin (G1), with thrombin aptamer-1 and aptamer-2 (G2), with aptamer-1 and thrombin (G3), with aptamer-2 and thrombin (G4), with aptamer-1 only (G5), with aptamer-2 only (G6), with thrombin only (G7), and without aptamers and thrombin (G8).

performed, and the results are consistent with the readout of electrical conductance.

Although SEM imaging allowed us to observe the surface of the polymeric sensor, the polymeric coating surrounding gNPs made it difficult to reveal clearly the biomolecular structure of the UPSS. AFM is highly sensitive in detecting subtle differences on the surfaces of various materials; therefore, it is possible to investigate the surface properties of the polymeric sensor during the polymeric network shrinkage triggered by target molecule binding. The adhesion and Log DMT Modulus images of AFM enable us to differentiate the gNPs from the polymeric network matrix using the stiffness and nonadhesion properties of gNPs. More importantly, the capability of AFM in quantitatively measuring normal and lateral forces at biomolecular levels makes it possible to study inter-biomolecular, intercellular and cell–molecule interactions.

To the best of our knowledge, the results reported here describe first attempt to use AFM to provide a direct measurement of the frictional forces between the probe tip and a polymer surface during polymeric network shrinkage triggered by biomolecular recognition. Indeed, the dose-dependent response of friction is fairly robust (Figure 5e). More importantly, these results are consistent with the data obtained using shrinkage measurements, electrical conductance measurements, or CLSM imaging upon biomolecular recognition as demonstrated above. These real-time in situ AFM measurements represent a novel approach for the precise measurement of biomolecules for nanosensing systems.

Collectively, the results reported here provide a proof-of-concept for a novel sensing system. Within the polymeric network, there might be complicated biomolecular interactions and events during biomolecular recognition and signal amplification; particularly, complex electrical and energy transporting process might be involved; consequently, it is difficult to use a classical theory for polymeric sensors to explain the exact mechanism of this novel sensing system. As such,

further investigation is warranted for a better understanding of the molecular mechanism of this novel sensor system. Again, the thrombin-specific or ATXa-specific UPSS demonstrated the possibility of creating a robust biofunctionalized polymeric sensing system. We anticipate that this system can be combined with microfluidics or array systems to fabricate high-throughput biomolecular recognition systems for environmental monitoring or clinical diagnostics.

Early detection of ultralow concentrations of circulating biomarkers or environmental toxins is of great importance for disease diagnosis and water safety monitoring which are vital to human's health. Given its high sensitivity and selectivity, this UPSS could potentially be used to detect early biomarkers in complex body fluid in chronic diseases such as cancer. For example, thrombin-specific UPSS could be used for accurate detection of urinary thrombin, which was found to be present in patients with glomerulonephritis or lupus nephritis.[21] Also, the UPSS possesses potential in monitoring the quality and safety of drinking water portably and rapidly. Furthermore, multiplex and high-throughput UPSS array might be designed and fabricated to suit the screening of multiple analytes. Finally, this system might be useful for ultrasensitive detection of various bioanalytes in a wide range of molecular weight.

Supporting Information

Supporting information is available from the Wiley Online Library or from the author.

Acknowledgements

This study was partly supported by a startup fund from the University of Houston (to T.W.) and a research grant from the Lupus Research Alliance (to T.W.). Additional support from the Robert A. Welch Foundation (T.R.L.; Grant No. E-1320) and the Texas Center for Superconductivity at the University of Houston (T.R.L.) is gratefully acknowledged.

Conflict of Interest

The authors declare no conflict of interest.

Keywords

biomolecular recognition, gold nanoparticles, polymeric biosensors, signal amplification

Received: April 13, 2017
Revised: May 5, 2017
Published online: June 14, 2017

[1] H. Craighead, *Nature* **2006**, *442*, 387.
[2] S. Ishihara, J. M. Azzarelli, M. Krikorian, T. M. Swager, *J. Am. Chem. Soc.* **2016**, *138*, 8221.
[3] H. D. Sikes, R. R. Hansen, L. M. Johnson, R. Jenison, J. W. Birks, K. L. Rowlen, C. N. Bowman, *Nat. Mater.* **2008**, *7*, 52.
[4] a) S. O. Kelley, C. A. Mirkin, D. R. Walt, R. F. Ismagilov, M. Toner, E. H. Sargent, *Nat. Nanotechnol.* **2014**, *9*, 969; b) H. Shao, J. Chung, L. Balaj, A. Charest, D. D. Bigner, B. S. Carter, F. H. Hochberg, X. O. Breakefield, R. Weissleder, H. Lee, *Nat. Med.* **2012**, *18*, 1835.
[5] J. Wang, *Electroanalysis* **2001**, *13*, 983.
[6] T. Miyata, M. Jige, T. Nakaminami, T. Uragami, *Proc. Natl. Acad. Sci. USA* **2006**, *103*, 1190.
[7] a) J.-M. Nam, C. S. Thaxton, C. A. Mirkin, *Science* **2003**, *301*, 1884; b) O. Knopfmacher, M. L. Hammock, A. L. Appleton, G. Schwartz, J. Mei, T. Lei, J. Pei, Z. Bao, *Nat. Commun.* **2014**, *5*, 2954; c) Y. Yan, S. C. Warren, P. Fuller, B. A. Grzybowski, *Nat. Nanotechnol.* **2016**, *11*, 603; d) H. Lee, T. K. Choi, Y. B. Lee, H. R. Cho, R. Ghaffari, L. Wang, H. J. Choi, T. D. Chung, N. Lu, T. Hyeon, *Nat. Nanotechnol.* **2016**, *11*, 566; e) E. Stern, A. Vacic, N. K. Rajan, J. M. Criscione, J. Park, B. R. Ilic, D. J. Mooney, M. A. Reed, T. M. Fahmy, *Nat. Nanotechnol.* **2010**, *5*, 138.
[8] P. Scrimin, L. J. Prins, *Chem. Soc. Rev.* **2011**, *40*, 4488.
[9] B. C. Tee, C. Wang, R. Allen, Z. Bao, *Nat. Nanotechnol.* **2012**, *7*, 825.
[10] a) M. A. C. Stuart, W. T. Huck, J. Genzer, M. Müller, C. Ober, M. Stamm, G. B. Sukhorukov, I. Szleifer, V. V. Tsukruk, M. Urban, *Nat. Mater.* **2010**, *9*, 101; b) Q. Zhou, T. M. Swager, *J. Am. Chem. Soc.* **1995**, *117*, 12593; c) Q. Zhou, T. M. Swager, *J. Am. Chem. Soc.* **1995**, *117*, 7017; d) Y. Yan, J. I. Chen, D. S. Ginger, *Nano Lett.* **2012**, *12*, 2530; e) L. Peng, M. You, Q. Yuan, C. Wu, D. Han, Y. Chen, Z. Zhong, J. Xue, W. Tan, *J. Am. Chem. Soc.* **2012**, *134*, 12302; f) W. Bai, D. A. Spivak, *Angew. Chem.* **2014**, *126*, 2127; g) W. Bai, N. A. Gariano, D. A. Spivak, *J. Am. Chem. Soc.* **2013**, *135*, 6977; h) L. Wang, L.-L. Li, H. L. Ma, H. Wang, *Chin. Chem. Lett.* **2013**, *24*, 351; i) C. Zhang, G. G. Cano, P. V. Braun, *Adv. Mater.* **2014**, *26*, 5678; j) L. Peng, C. S. Wu, M. You, D. Han, Y. Chen, T. Fu, M. Ye, W. Tan, *Chem. Sci.* **2013**, *4*, 1928; k) R. J. Amir, E. Danieli, D. Shabat, *Chem. - Eur. J.* **2007**, *13*, 812; l) A. Sagi, R. Weinstain, N. Karton, D. Shabat, *J. Am. Chem. Soc.* **2008**, *130*, 5434; m) S. T. Phillips, A. M. DiLauro, *ACS Macro Lett.* **2014**, *3*, 298.
[11] O. Veiseh, B. C. Tang, K. A. Whitehead, D. G. Anderson, R. Langer, *Nat. Rev. Drug Discovery* **2015**, *14*, 45.
[12] a) P. H. Kouwer, M. Koepf, V. A. Le Sage, M. Jaspers, A. M. van Buul, Z. H. Eksteen-Akeroyd, T. Woltinge, E. Schwartz, H. J. Kitto, R. Hoogenboom, *Nature* **2013**, *493*, 651; b) N. Dave, M. Y. Chan, P.-J. J. Huang, B. D. Smith, J. Liu, *J. Am. Chem. Soc.* **2010**, *132*, 12668; c) B. P. Purcell, D. Lobb, M. B. Charati, S. M. Dorsey, R. J. Wade, K. N. Zellers, H. Doviak, S. Pettaway, C. B. Logdon, J. Shuman, *Nat. Mater.* **2014**, *13*, 653; d) D. J. Beebe, J. S. Moore, J. M. Bauer, Q. Yu, R. H. Liu, C. Devadoss, B.-H. Jo, *Nature* **2000**, *404*, 588.
[13] H.-A. Ho, M. Leclerc, *J. Am. Chem. Soc.* **2004**, *126*, 1384.
[14] a) W. H. Hudson, E. A. Ortlund, *Nat. Rev. Mol. Cell Biol.* **2014**, *15*, 749; b) M. Jing, M. T. Bowser, *Anal. Chim. Acta* **2011**, *686*, 9; c) H. Xing, N. Y. Wong, Y. Xiang, Y. Lu, *Curr. Opin. Chem. Biol.* **2012**, *16*, 429; d) W. Yi-Xian, Y. Zun-Zhong, S. Cheng-Yan, Y. Yi-Bin, *Chin. J. Anal. Chem.* **2012**, *40*, 634.
[15] S. Patel, H. Park, P. Bonato, L. Chan, M. Rodgers, *J. Neuroeng. Rehabil.* **2012**, *9*, 1.
[16] Y. Kim, J. Zhu, B. Yeom, M. Di Prima, X. Su, J.-G. Kim, S. J. Yoo, C. Uher, N. A. Kotov, *Nature* **2013**, *500*, 59.
[17] D. G. Castner, K. Hinds, D. W. Grainger, *Langmuir* **1996**, *12*, 5083.
[18] Y. Mao, Y. Bao, S. Gan, F. Li, L. Niu, *Biosens. Bioelectron.* **2011**, *28*, 291.
[19] a) S. Viswanathan, C. Rani, S. Ribeiro, C. Delerue-Matos, *Biosens. Bioelectron.* **2012**, *33*, 179; b) D. Cai, L. Ren, H. Zhao, C. Xu, L. Zhang, Y. Yu, H. Wang, Y. Lan, M. F. Roberts, J. H. Chuang, *Nat. Nanotechnol.* **2010**, *5*, 597.
[20] a) J. Das, K. B. Cederquist, A. A. Zaragoza, P. E. Lee, E. H. Sargent, S. O. Kelley, *Nat. Chem.* **2012**, *4*, 642; b) Y. Xiang, M. Xie, R. Bash, J. J. Chen, J. Wang, *Angew. Chem., Int. Ed.* **2007**, *46*, 9054; c) V. Pavlov, Y. Xiao, B. Shlyahovsky, I. Willner, *J. Am. Chem. Soc.* **2004**, *126*, 11768.
[21] Y. Kitamoto, K. Arizono, H. Fukui, K. Tomita, H. Kitamura, Y. Taguma, T. Imamura, *PLoS One* **2015**, *10*, e0118704.